Clumped isotope paleotemperatures from MIS 5 stage soil carbonates in southern Hungary

Gábor Újvári[a*], Sándor Kele[a], Stefano M. Bernasconi[b], László Haszpra[c,d], Ágnes Novothny[e], Balázs Bradák[f,g]

[a]Institute for Geological and Geochemical Research, Research Centre for Astronomy and Earth Sciences, Hungarian Academy of Sciences, Budaörsi u. 45, H-1112 Budapest, Hungary
[b]Geological Institute, ETH Zürich, Sonneggstrasse 5, 8092 Zürich, Switzerland
[c]Hungarian Meteorological Service, Kitaibel Pál u. 1., H-1024 Budapest, Hungary
[d]Geodetic and Geophysical Institute, Research Centre for Astronomy and Earth Sciences, Hungarian Academy of Sciences, Csatkai E. u. 6-8., H-9400 Sopron, Hungary
[e]Department of Physical Geography, Eötvös Loránd University, Pázmány Péter sétány 1/c, H-1117 Budapest, Hungary
[f]Independent Researcher
[g]Research Center for Inland Seas, Kobe University, Nada, Kobe, 657-8501, Japan

*Corresponding author: G. Újvári, Email: ujvari.gabor@csfk.mta.hu
Present address: Department of Lithospheric Research, University of Vienna
Althantrsasse 14 (UZA II), 1090 Vienna, Austria

Abstract

Quantitative paleotemperature reconstructions for the continents, including East Central Europe, over marine isotope stage 5 (MIS 5) and specifically the last interglacial (LIG, MIS 5e) are scarce and mostly based on pollen assemblages. Here we provide soil and air temperature reconstructions for the summer season of MIS 5e (5c) using carbonate clumped isotope thermometry applied to soil carbonate concretions in the Dunaszekcső loess-paleosol record, Southern Hungary. The sediments making up the S1 pedocomplex investigated represent the MIS 5 as demonstrated by bracketing K-feldspar post IR-IRSL$_{225/290}$ ages of ~63 to 164 ka. Both the absolute ages and pedogenic susceptibility (χ_P) curve indicate that all the subtages of MIS 5 were found to be recorded in the sequence, and soil carbonates found >1 m depth below the paleosurface of the S1 soil provide pristine, undisturbed isotopic signals. The soil carbonate concretions likely formed during MIS 5e at a relatively shallow (20-50 cm) depth, but a later formation during MIS 5c at >50 cm depth is also plausible. Clumped isotope-based soil temperatures (ST-Δ_{47sc}) ranged from 16 to 20 ºC, and reconstructed summer season air temperatures (SATs) for the LIG are consistently lower than the modern values at the site by 1−5 ºC, matching surprisingly well the soil bacteria membrane lipid-based MIS 5e air temperature estimates from a nearby Serbian site. At the same time, the reconstructed SAT values do not match the 2−4 ºC positive warm season anomalies modeled for East Central Europe between LIG and present-day in paleoclimate simulations. ST uncertainties of 1−6 ºC, infiltration-driven cooling of soil temperatures, and the possibility of MIS 5c formation of the investigated carbonates may account for this proxy-model data discrepancy. Oxygen isotope compositions of summer season paleo-rainwaters for MIS 5e (5c), as reconstructed using the ST-Δ_{47sc} and $\delta^{18}O_{sc}$ data of soil carbonates, were found in a range of −6.7 and −6.4 ‰, matching the modern mean summer season value of −6.2±0.94 ‰ within error.

Keywords: marine isotope stage 5; loess-paleosol; soil carbonate nodule; oxygen isotope; ^{13}C-^{18}O bonding; Δ_{47}

1. Introduction

The last interglaciation (LIG, ~130−115 ka), the most recent warm period in Earth's climate history prior to the Holocene (0−12 ka), was characterized by reduced terrestrial ice volume and higher-than-modern global sea level (EPICA community members, 2004; Lisiecki and Raymo, 2005; Kopp et al., 2009; NEEM community members, 2013). Marine and terrestrial proxy data indicate a global mean warming of ~1.5 ºC during the LIG, corresponding to Marine Isotope Stage 5e (MIS 5e), relative to today (Turney and Jones, 2010), and an increase of global mean sea surface temperature of 0.7±0.6 ºC relative to the late Holocene (McKay et al., 2011). The maximum annual mean and summer temperature anomalies reached 4−5 ºC in high Northern Hemisphere latitudes (CAPE-Last Interglacial Project Members, 2006; Capron et al., 2014). Natural variations in greenhouse gases (CO_2 and CH_4 maximum between 129-128 ka; Lüthi et al., 2008; Loulergue et al., 2008) played a significant role in warming, while the other driver of climatic differences between the LIG and modern climate is the astronomical configuration of Earth (Yin and Berger, 2010). During the early LIG, precession minima (boreal summer at perihelion) and obliquity maxima were in-phase, amplifying Northern Hemisphere (NH) insolation (Past Interglacials Working Group of PAGES, 2016).

Subsequent insolation-driven climate ameliorations over MIS 5, such as MIS 5c and 5a, were characterized by ~2 ºC lower global sea surface temperatures (SSTs) (Shakun et al., 2015) and ~3−4 ºC lower summer SSTs in the subpolar North Atlantic (Oppo et al., 2006) compared to MIS 5e. Climate of the MIS 5 stage was punctuated by several, millennial scale cold intervals as recorded in marine sediments of the North Atlantic (McManus et al., 1994), ice cores in Greenland (Rasmussen et al., 2014; Kindler et al., 2014) and speleothems in the European Alps (Boch et al., 2011). While all the forested intervals of MIS 5 (5e, c, a) were characterized by mild climate, the last interglacial (MIS 5e) was the most temperate period, as shown by pollen records and Coleoptera assemblages, and the MIS 5c and 5a intervals had more continental climate regimes both in western (Guiot et al., 1992, 1993, Cheddadi et al., 1998) and central Europe (Granoszewski, 2003; Klotz et al., 2004; Behre et al., 2005; Kühl et al., 2007; Helmens, 2014).

While the LIG cannot be considered as an analogue for future climate change due to different forcing mechanisms, it is still an appropriate period to test climate models under warmer-than-present conditions (Lunt et al., 2013; Nikolova et al., 2013). Robust LIG model-data comparisons are particularly important to test models developed for future climate projections. The existing LIG paleo-data syntheses are mostly dominated by marine sea surface temperature records and continental temperatures are mainly derived from ice core and pollen records (Kaspar et al., 2005; Turney and Jones, 2010; McKay et al., 2011). To improve these datasets and facilitate model-data comparisons further quantitative temperature estimations are required from other, well-dated continental archives. European loess-paleosol sequences often provide a record of MIS 5, including the LIG, but these have remained largely underutilized so far due to poor dating and a lack of reliable temperature proxies. Most studies provided information on weathering and pedogenesis from LIG paleosols (S1) using magnetic indicators (Buggle et al., 2009, 2014; Marković et al., 2011; Fitzsimmons et al., 2012; Zeeden et al., 2016; Sümegi et al., 2018), grain size (Novothny et al., 2011; Stevens et al., 2011; Terhorst et al., 2012; Antoine et al., 2013; Sprafke et al., 2014) and chemical proxies (Buggle et al., 2013; Galović, 2014; Hošek et al., 2015; Obreht et al., 2016). At the same time, quantitative vegetation, rainfall and temperature reconstructions (Panaiotu et al., 2001; Zech et al., 2013; Schreuder et al., 2016; Marković et al., 2018) are scarce and sometimes inconsistent. For instance, while Zech et al. (2013) concluded that MIS 5 warm periods were more arid at the Crvenka site with the expansion of grasses, Schreuder et al. (2016) have found the opposite at Surduk in terms of precipitation (both sites in Serbia).

Based on membrane lipids (branched glycerol dialkyl glycerol tetraethers, brGDGTs) of soil bacteria, wet/warm conditions were reconstructed for MIS 5 at Surduk, with decreasing temperatures from ~18−20 (MIS 5e) to 16 ºC (MIS 5a) (Schreuder et al., 2016). Since these temperatures were found to be well above the present-day mean annual air temperature (MAT, ~11 ºC) at the study site, they were interpreted as being seasonal (likely summer) air temperatures.

This study provides quantitative soil temperature (ST) and air temperature estimates from the oxygen and clumped isotope compositions of soil carbonates developed during MIS 5 in the S1 paleosol of the Dunaszekcső loess record in Southern Hungary. The oxygen isotope composition of soil carbonate ($\delta^{18}O_{sc}$) depends on ancient meteoric water $\delta^{18}O$ and the temperature of carbonate formation (Cerling, 1984; Cerling and Quade, 1993). Therefore, to obtain robust paleo-temperature estimates independent assumptions on ancient precipitation oxygen isotopic compositions ($\delta^{18}O_{prec}$) are required. Clumped isotope thermometry offers a solution as it is based on the temperature-dependent formation of ^{13}C−^{18}O bonds in carbonate minerals, providing the formation temperature of carbonates (Ghosh et al., 2006; Eiler, 2007, 2011). Using the simultaneously measured $\delta^{18}O_{sc}$ this approach allows the calculation of $\delta^{18}O$ of meteoric water. However, seasonal biases in soil carbonate formation are complex (Huntington and Lechler, 2015), and the isotopic composition of carbonates may reflect annual, spring/fall or even winter season (Peters et al., 2013; Gallagher and Sheldon, 2016), and also summer season signals (Breecker et al., 2009; Passey et al., 2010; Quade et al., 2013; Hough et al., 2014; Burgener et al., 2016, 2018), depending on a number of factors such as soil temperature, moisture, evaporation, pH and CO_2 concentration (Huntington and Lechler, 2015). Due to all these uncertainties, the seasonal bias in carbonate formation is tested and evidence is provided that the S1 soil carbonate Δ_{47}-temperatures (ST-Δ_{47sc}) are representative of mean warm/summer season soil and air temperatures (SAT). Carbonate formation depths and timings together with the S1 soil development are also discussed in detail in the light of magnetic susceptibility and stable isotope data. Thus, our study provides quantitative ST and SAT estimates together with ancient meteoric water $\delta^{18}O$, and pedogenic susceptibility-based mean annual precipitation (MAP) reconstructions in southern Hungary for MIS 5. Further, our ST-Δ_{47sc} data are discussed in the context of instrumental soil/air temperature measurements at the Szeged meteorological station.

2. Materials and methods

2.1. Settings and site information

The studied loess-paleosol section is located at Dunaszekcső, Southern Hungary (Fig. 1), on the right bank of the Danube river (46º05'25"N, 18º45'45"E, 135 m a.s.l.) and exposes glacial-interglacial sediments. A detailed lithostratigraphic description of the profile can be found in Újvári et al. (2014). In 2008, an enormous bank failure exposed the uppermost ~17 m part of the ca. 70 m thick Quaternary loess–paleosol sequence at Dunaszekcső (Újvári et al., 2009), thereby allowing the sampling of a relatively fresh profile.

This part of the Carpathian Basin is an area of low relief between the main mountain ranges of central Europe and is under Atlantic, Mediterranean, and continental climatic influence. This is expressed in the amount of annual rainfall (575 $mm \cdot y^{-1}$, with extremes of 276 $mm \cdot y^{-1}$ to 882 $mm \cdot y^{-1}$) and mean air temperatures during winter (1.0 °C, Dec−Jan) and summer (21.5 °C, June−Aug) as measured at a nearby located meteorological station (Sátorhely, Fig. 1) for the period 1998–2013.

Since soil temperature (ST) data were not available for the Dunaszekcső site and Sátorhely station, ST data measured at the Szeged meteorological station are used and reported in this study. The Szeged station is located at the same latitude on the Great Hungarian Plain, ~103 km east to the Dunaszekcső site. Both regions have similar climate

(Fig. 1) and the parent material of chernozem soils at the Szeged station is loess. Therefore, the ST data recorded at the Szeged station as a function of depth and air/soil temperature relations are considered representative for the Dunaszekcső site.

2.2. Absolute dating, magnetic susceptibility measurements and paleoprecipitation reconstructions

After cleaning of the sediment surface in the profile, altogether 5 samples were collected for infra-red stimulated luminescence dating of potassium-feldspars (Thomsen et al., 2008; Buylaert et al., 2009) at various depths in and around the pedocomplex overlying the L2 loess unit corresponding to Marine Isotope Stage (MIS) 6 (Újvári et al., 2014). This was done by pushing metal tubes into the loess-paleosols. Additional sediment samples from around the luminescence sampling holes were taken for gamma spectrometry. Further details on the methodology of both the post-IR IRSL dating (225/290 ºC) and gamma spectrometry protocols applied in this study can be found in Újvári et al. (2014).

Samples for magnetic susceptibility measurements were collected at 5 cm (depth: 12.85−12.05 m) and 2 cm (depth: 14.57−12.85 m) resolution (Supplementary Dataset 1). Mass-specific magnetic susceptibility (χ) was measured at two operating frequencies (0.47 and 4.7 kHz) using an MS2B Dual Frequency Sensor linked to a Bartington Ltd. MS3 Susceptibility Bridge. Sample powders were filled in 10 ml plastic containers and empty container and sample masses were measured using a Kern PCB 250-3 high precision balance (reproducibility: ±0.001 g). The absolute frequency-dependent susceptibility, $\chi_{FD} = \chi_{LF} - \chi_{HF}$, reflects the concentration of magnetic particles over a small grain size window across the superparamagnetic (SP)/stable single domain (SSD) boundary (Liu et al., 2012). By changing the observation time (i.e. frequency) a fraction of SSD grains turns superparamagnetic at a decreased frequency causing a sharp increase in magnetic susceptibility (Maher, 1986;

Dearing et al., 1996; Worm, 1998). These grains form *in situ* in soils during pedogenesis (Maher and Taylor, 1988; Zhou et al., 1990), thus χ_{FD} is considered as a proxy of pedogenesis (Heller et al., 1993; Maher and Thompson, 1995; Buggle et al., 2014). To calculate the magnetic susceptibility contribution from SP/SSD particles, called the pedogenic susceptibility ($\chi_P = \chi_{LF} - \chi_B$), we used an χ_{LF} vs. χ_{FD} diagram to estimate the background susceptibility (χ_B) representing the eolian detrital input (Forster et al., 1994). From this diagram $\chi_B = 1.56365 \times 10^{-7}$ m^3 kg^{-1} (Fig. S1) and χ_P can be calculated, which records pedogenesis quantitatively (Forster et al., 1994).

For the estimation of MAP (Supplementary Dataset 1), the equation of Maher et al. (1994)

$$MAP\ (mm\ yr^{-1}) = 222 + 199\ log_{10}\chi_P \qquad (1)$$

was used, obtained on modern soils in China. Uncertainties of MAP reconstructions are estimated to be in the range of 2–5% according to the sensitivity analysis performed by Maher et al. (1994). This approach was successfully applied to both modern soils and paleosols by Panaiotu et al. (2001) and Bradák et al., (2011).

2.2. Stable- and clumped isotopic analyses

For the separation of carbonate concretions 15 cm thick sediment blocks were prepared and cut from the S1 paleosol (Table 1), which were subsequently disintegrated in the lab by soaking in distilled water. The concretions were extracted by washing the sediments through a sieve, then dried at 50 ºC and finally cut into two pieces using a diamond saw. Internal textures of concretions were examined under microscope and micritic calcite (Fig. S2) was exclusively sampled for stable and clumped isotope analyses.

All carbonate samples were powdered and homogenized using an agate mortar and pestle. Carbon and oxygen isotope analyses of bulk carbonate samples were carried out at

ETH Zürich (Zürich, Switzerland) as part of the clumped isotope analyses with a Thermo Fisher Scientific Kiel IV preparation device coupled to a Thermo Fisher Scientific MAT 253 isotope ratio mass spectrometer, as described by Schmid and Bernasconi (2010) with improvements, including a carbonate-based correction scheme presented by Meckler et al. (2014), Müller et al. (2017) and Bernasconi et al. (2018). Instead of using heated and equilibrated gases, at ETH the procedures for determining Δ_{47} in the absolute reference frame (ARF; Dennis et al., 2011) include: (1) pressure baseline correction of the raw beam intensities according to Bernasconi et al. (2013); (2) calculation of the Δ_{47} values with respect to the working gas of the mass spectrometer; (3) conversion to the ARF by a transfer function determined by plotting the measured vs. the accepted values of carbonate standards ETH-1 to ETH-4; (4) correction for the phosphoric acid fractionation difference between 70 and 25°C (0.062%). The data were calculated using the "Brand parameters" for the ^{17}O corrections as suggested by Daëron et al. (2016) and Schauer et al. (2016), and normalized to the reference frame using the revised accepted composition of the ETH-1 to ETH-4 standards reported in Bernasconi et al. (2018) (Supplementary Datasets 2 and 3).

Traditional stable carbon and oxygen isotope compositions and clumped isotope composition were calculated as the average of 7–9 replicate analyses of 120 − 180 µg of carbonate. The stable carbon and oxygen isotope ratios are reported in the conventional δ notation in per mil (‰) relative to the Vienna Pee Dee Belemnite (VPDB) as: $\delta_{sample} = (R_{sample} / R_{VPDB}) - 1$, where R is $^{13}C/^{12}C$ for carbon and $^{18}O/^{16}O$ for oxygen (Coplen et al., 1994). The temperature-dependent mass 47 anomaly is defined as (Ghosh et al., 2006)

$$\Delta_{47}(‰) = \left[\left(\frac{R^{47}}{R^{47*}} - 1\right) - \left(\frac{R^{46}}{R^{46*}} - 1\right) - \left(\frac{R^{45}}{R^{45*}} - 1\right)\right] \times 1000 \quad (2)$$

where R^i is the abundance of the minor isotopologues relative to the most abundant isotopologue with mass 44, and the expected stochastic ratios R^{i*} are calculated based on the measured abundance of ^{13}C and ^{18}O in the sample. The results are reported in the absolute reference frame (Dennis et al 2011).

2.3. Calculations and modeling related to stable/clumped isotope compositions

ST-Δ_{47sc} values (in ºC) were calculated from clumped isotope compositions (Δ_{47}) of soil carbonates using the travertine-based Δ_{47}-temperature calibration (Kele et al., 2015), recalculated with the new Brand parameters (Breitenbach et al., 2018; Bernasconi et al., 2018). The Kele et al. (2015) calibration is used in this study, as it was produced using the same analytical techniques at ETH Zürich (Zürich, Switzerland), thus ensuring internally consistent data processing and standardisation. Summer season air temperatures (SATs in ºC) were estimated using measured mean air (2 m) and soil temperatures at 1, 0.5 and 0.2 m for the summer season at the Szeged station, as given in section 3. Two independent methods were adopted for MAT calculations: 1) the first one used $\delta^{18}O_{sc}$ and

$$MAT(°C) = (\delta^{18}O_{sc} + 12.65)/0.49 \quad (3)$$

as given by Dworkin et al. (2005), and 2) the method and

$$MAT(°C) = 1.20 \times T°C(47)_0 - 21.72 \quad (4)$$

published in Quade et al. (2013). Warmest average monthly air temperature was also calculated after Quade et al. (2013) using

$$WMAT(°C) = 1.13 \times T°C(47)_0 - 10.81 \quad (5)$$

To infer the "effective surface temperature", or $T°C(47)_0$, a summer season soil temperature profile was modeled and fitted to the ST-Δ_{47sc} data by minimizing the sum of squared errors/residuals. Simulation of summer soil temperatures as a function of depth is based on Hillel (2003) and Quade et al. (2013)

$$T(z,t) = T_{avg} + A_0[\sin(\omega t - z/d)]e^{-z/d} \quad (6)$$

, with model parameters defined in Table 2.

Paleoprecipitation oxygen isotopic compositions ($\delta^{18}O_{prec}$) were calculated from $\delta^{18}O_{sc}$ and ST-Δ_{47sc} data using the calcite-water oxygen isotope fractionation equation

$$1000 ln\alpha_{(calcite-water)} = 18.03 \times (10^3 T^{-1}) - 32.42 \qquad (7)$$

of Kim and O'Neil (1997).

3. Results and discussion

3.1. Soil and air temperature relationship at the Szeged station

Mean soil temperatures at shallow depths (average of 6 consecutive years) closely follow annual air temperature variations at the Szeged meteorological station (Fig. 2a), while those at 0.5 m and 1.0 m depths are, as expected, shifted in time and the maximum/minimum temperatures are damped (Hillel, 2003). Observed soil temperatures at shallow depths (0.1 and 0.2 m) higher than air temperature at 2 m during the summer season are due to ground heating by incident solar radiation (Quade et al., 2013). This effect causes shallow soil temperatures to be ~2.0 ºC in excess of SAT at the Szeged station.

Since the analyzed soil carbonates from the Dunaszekcső sequence may have formed at shallower depths compared to the paleosurface than their present position recorded during sample collection (Table 1; discussion in section 3.3) and during the summer season (see later in section 3.2), the relationships between modern mean SAT and summer soil temperatures (SST) at 1, 0.5 and 0.2 m depths were investigated. Analysis of our datasets yield a set of linear equations for these depths (1, 0.5 and 0.2 m, Fig. 2b):

$$y = 1.29(\pm 0.18)x - 3.21(\pm 3.42) \qquad (8)$$

R=0.96 (p=0.001963, p(a) < 0.01, n=6)

$$y = 0.98(\pm 0.20)x + 0.55(\pm 4.26) \qquad (9)$$

R=0.93 (p=0.008011, p(a) < 0.01, n=6)

$$y = 0.78(\pm 0.22)x + 3.57(\pm 5.04) \qquad (10)$$

R=0.87 ($p=0.023671$, $p(a) < 0.05$, $n=6$)

, where the independent (x) and dependent (y) variables are SST and SAT (in ºC), respectively. Thus, SATs are found to be consistently higher than SSTs at 1 m depth by ~1 to 3 ºC at the Szeged station. Due to less thermal damping SAT values are close to SSTs at 0.5 m depth (slope=~1, Eq. 9), while SATs are lower than SSTs by ~1.5−3 ºC at 0.2 m depth. Further testing of these relationships is required at other sites with soils developed on loess parent material, as drier regions with sparse vegetation may have different relationships due to stronger ground heating effect. Although it cannot be directly tested, in this study we assume that the modern SST-SAT relationships are valid for the warm phases of MIS 5 (especially MIS 5e) because of the generally similar climate (seasonality of rainfall and temperatures) and vegetation cover (Harrison et al., 1995; Helmens, 2014).

3.2. Soil carbonate stable and clumped isotope compositions and soil/air temperature reconstructions

Carbon and oxygen isotopic compositions of soil carbonates ($\delta^{13}C_{sc}$, $\delta^{18}O_{sc}$) from the S1 paleosol are confined to ranges of −9.41 to −8.87 ‰ (SE: 0.02-0.05) and −7.78 to −7.19 (SE: 0.03-0.08) ‰, with the highest $\delta^{18}O_{sc}$ value recorded in the uppermost nodule in the soil profile (Table 1; Fig. 3). These carbon isotope values are overlapping, while the oxygen isotope compositions are ~ 1−2 ‰ less negative than those measured in concretions of last interglacial soils in sequences at Süttő (Königer et al., 2014) and Verőce (Barta et al., 2018), ~250 km north of the study site. Soil temperatures calculated from the clumped isotope compositions (ST-Δ_{47sc}) were found in a broad range (3 to 20 ºC, with 1.3-6.1 ºC uncertainty; Table 1), with two extreme values (Dsz-SC-1 and 10/1, Table 1, Fig 3a). The ST value of 2.7 ºC (Dsz-SC-10/1) is considered to be an outlier, while the lower ST value (10.4 ºC) recorded in the Dsz-SC-1 nodule may simply reflect a different season of formation. Due to shallow formation depth, carbonate precipitation could be biased to soil drying after small, frequent precipitation events occurring throughout the spring, summer, and fall months (Ringham et al., 2016). So, this is probably an annual signal as the SAT value (11.7 ºC, calculated with Eq. 10 for 0.2 m depth) coincides with the modern MAT (11.6 ± 0.7 ºC) of this region (Fig. 1). Nodules at depths of 1.05−1.50 m record ST values of 16.5 to 19.9 ºC, overlapping summer season STs measured at 1 m depth at the Szeged station (15.6−21.8 ºC; 19.1 ± 1.7 ºC) and the simulated modern summer season STs (Fig. 3a).

SAT values estimated by Eqs. (8) range between 18.1 and 22.4 ºC (Table 1), corresponding with the present-day range of summer season temperatures (~20−22.5 ºC). The "effective surface temperature" $T^{o}C(47)_0$ is 22.0 ºC, as given by the intersect of the best-fit model curve (green line, Fig. 3a) and the surface. Both the warmest average monthly and mean annual air temperatures (WAMT/MAT), calculated using $T^{o}C(47)_0$, were found to be unrealistically low (14.1 and 4.7 ºC) for this region. This implies that the equations (Eqs. 3-4) by Quade et al. (2013) indeed do not seem to be universal, as proposed by the authors. MAT estimates using the Dworkin et al. (2005) equation (Eq. 2) gave slightly lower values (9.9−11.1 ºC; Table 1) than the modern value (11.6 ºC). These figures seem to be correct despite the fact that the $\delta^{18}O_{sc}$ compositions of the investigated carbonates (>50 cm depth) reflect the summer season, and are not annual signals (see below).

Using soil nodule ST-Δ_{47sc} and $\delta^{18}O_{sc}$ data, the reconstructed oxygen isotopic compositions of the paleoprecipitation ($\delta^{18}O_{prec}$) were found in a range of −6.72 to −6.45 (Table 1), excluding samples Dsz-SC-1 and 10/1. We could not find any indication of analytical problems or contamination with these two samples. For Dsz-SC-1, the lower ST-Δ_{47sc} and $\delta^{18}O_{prec}$ values can be accounted for by a spring-fall bias in carbonate formation, and/or a bias to soil drying after small, frequent precipitation events (averaging to shallow summer ST-Δ_{47sc}) due to a shallow formation depth (Ringham et al., 2016). At the same time, for Dsz-SC-10/1 the possibility of the isotopic signature being altered through diagenesis or contamination cannot be excluded. Therefore, these two samples were not used in $\delta^{18}O_{prec}$ reconstructions.

The mean seasonal $\delta^{18}O_{prec}$ values as measured at the closest (Zagreb) GNIP station for the period of 1980-1995 are shown in Fig. 4 as a function of mean seasonal air temperatures, together with the reconstructed $\delta^{18}O_{prec}$ values from soil carbonates (>1 m depth) at the Dunaszekcső S1 soil. The range of reconstructed $\delta^{18}O_{prec}$ values (−6.7 to −6.4 ‰; Table 1) are very close to the summer season mean (−6.2±0.94 ‰) of the Zagreb GNIP station. Only some unusually heavy oxygen isotope compositions of the spring season were found to be overlapping the reconstructed $\delta^{18}O_{prec}$ values of the S1 soil carbonates. Therefore, we interpret the ST-Δ_{47sc} values of the S1 soil carbonates (>1 m depth) as being representative of the summer season.

3.3. Absolute chronology and correlations, paleosol and soil carbonate development in MIS 5 and paleotemperature reconstructions

The sediments making up the paleosol complex in the Dunaszekcső section were formed during MIS 5, as indicated by the K-feldspar post IR-IRSL ages obtained in the profile (Table 3; Fig. 5a). These absolute ages, together with the magnetic susceptibility curve demonstrate an accretionary soil development and that all the MIS 5 substages (e to a) seen in the LR04 $\delta^{18}O_{benthic}$ curve are recorded in the sequence. MIS 5e (=LIG) and MIS 5c are characterized by intense pedogenesis (χ_P curve peaks; Fig. 5c), while the intensity of soil formation was much reduced during MIS 5a. After the cold MIS 6 period, significant warming commenced in this region at ~129−130 ka, as demonstrated by the >3 ‰ positive shifts in speleothem carbonate $\delta^{18}O$ values in the nearby Abaliget cave (Koltai et al., 2017). Estimated mean annual precipitation (MAP) reached ~620−630 mm in MIS 5e and 5c, with a significant drop during MIS 5b (~480 mm) and still low values (~510 mm) in MIS 5a (Fig. 5c).

Both paleopedological and magnetic susceptibility data indicate that two separate phases of intense pedogenesis occurred and are seen in the S1 paleosol (Fig. 5c), and the soil carbonate concretions may have formed in any of these periods. Accordingly, soil nodules originate from >1 m depth in the paleosol profile (from the paleosurface) may have precipitated during MIS 5e or 5c. Both scenarios are plausible in lack of direct U−Th dating of soil carbonate concretions. Provided that the nodules (>1 m depth) were formed during MIS 5e, the carbonate precipitation depth may have ranged between 20−50 cm from the paleosurface. If later (MIS 5c), the nodules could have formed at >50 cm (mostly 60−100 cm) depth. In this case, these authigenic soil carbonates would have formed during MIS 5c at a soil depth that corresponds to soil/loess that was originally deposited during MIS 5e. Both scenarios are discussed below. As for the soil carbonate collected at a shallow depth (Dsz-SC-1, Table 1), this nodule may have precipitated at the end of MIS 5c or during MIS 5a.

According to scenario 1 (MIS 5e formation), the soil carbonates reflect LIG (MIS 5e) summer season soil/air temperatures and rainfall oxygen isotope compositions. The reconstructed ST-Δ_{47sc} values would correspond to 20−50 cm soil depth and the calculated (Eq. 9) SAT values would be ~4−1.5 ºC below modern summer air temperatures (Table 1). Interestingly, the reconstructed SAT values (17−20 ºC, Table 1) correspond to MIS 5e paleotemperature estimates from brGDGTs in the Surduk loess-paleosol sequence (Fig. 5b), Serbia, 200 km to the south of our study site (Schreuder et al., 2016). Our ST-Δ_{47sc} dataset, therefore, supports the hypothesis by Schreuder et al. (2016) that brGDGT-based temperatures in loess/soil profiles in Europe record summer season temperatures instead of mean annual temperatures, similarly to Chinese loess deposits (Peterse et al., 2011).

Last interglacial paleoclimate simulations modeled 0.5−2 ºC higher MATs for East Central Europe than the modern values (McKay et al., 2011; Lunt et al., 2013; Otto-Bliesner et al., 2013). Simulated summer season air temperature anomalies between the LIG and present-day are mostly in the range of +2 – +4 ºC for East Central Europe (Kaspar et al., 2005; Bakker et al., 2013; Nikolova et al., 2013), but even higher (+4 – +6 ºC) June-July-August temperature anomalies were found in some models (Otto-Bliesner et al., 2013). Our $\delta^{18}O_{sc}$-based MAT estimates are slightly (~<1 ºC) lower than the modern value in the study region. Likewise, the SAT values obtained in our study and in Schreuder et al. (2016) both indicate a negative temperature anomaly of 1−5 ºC for the LIG warm season (Fig. 5b). These proxy-based negative MAT and SAT anomalies for the LIG are in contrast to the positive anomalies modeled for East Central Europe. To reconcile this contradiction we have three explanations. First, the uncertainties associated with ST-Δ_{47sc} values range from ~1 to 6 ºC must be considered. Second, the lower ST-Δ_{47sc} values are possibly due to the relatively shallow (20−50 cm) formation depths, and the almost isothermal ST-Δ_{47sc} values may indicate infiltration-driven cooling of soil temperatures. In this situation carbonate formation later in the drying curve (back to baseline conditions) would result in lower ST-Δ_{47sc} values than the real values at all depths (see Ringham et al. 2016). Third, the later (MIS 5c) formation of soil carbonates cannot be dismissed. Indeed, if the soil nodules are authigenic (scenario 2), they simply reflect summer season temperatures of MIS 5c, which was a generally slightly colder period than MIS 5e (Fig. 5d-f; McManus et al., 1994; Shakun etal., 2015). In this case, the SAT values of 18.1 to 22.4 ºC (Eq. 8, Table 1), would correspond to the modern value (21.5±1.6 ºC). Therefore, further quantitative paleodata and systematic, preferably combined brGDGT/soil carbonate clumped isotope studies on MIS 5 paleosols are needed to better understand both proxies and validate model results.

4. Conclusions

The paleosol complex in the Dunaszekcső loess-paleosol sequence, dated by the K-feldspar post IR-IRSL method, is formed during MIS 5. All subtages of MIS 5 seem to be recorded in the sediments as demonstrated by the luminescence ages and the pedogenesis proxy (χ_P data). Soil carbonates at >1 m depths in the lower paleosol may have formed during the summer season of MIS 5e or 5c, while the one sampled at shallow depth could have precipitated at the end of MIS 5c or 5a in the spring-to-fall seasons. Soil carbonates (>1 m depth) yielded soil temperatures (ST-Δ_{47sc}) of 17 to 20 ºC (sample Dsz-SC-10/1 excluded), which translates into SAT values of 17 to 20 ºC, provided that they formed in MIS 5e at a depth of 20−50 cm. These carbonate clumped isotope temperatures, recorded in the Dunaszekcső sequence, match surprisingly well the brGDGT-based paleotemperature estimates (16−19 ºC) for the MIS 5e period at the Surduk site in Serbia, 200 km to the south. These reconstructed SATs are by 1−5 ºC lower than the modern value and do not match the simulated LIG/present-day temperature anomalies for the warm season in East Central Europe, which usually range from +2 to 4 ºC in most LIG model simulations. However, the ST-Δ_{47sc} values are associated with 1−6 ºC uncertainties (2σ), and the possibility of soil nodule formation during the MIS 5c period cannot be excluded in lack of direct U−Th dating on these carbonates.

Clumped isotope temperatures and soil carbonate concretion oxygen isotope compositions allowed for reconstructing the $\delta^{18}O$ of past rainfall, interpreted as an integrated signal of the summer season. Precipitation oxygen isotope compositions were found to be more negative (by ~0.5 ‰) than the modern value (−6.2±0.94 ‰) measured at the closest GNIP station (Zagreb). In fact, these paleo-$\delta^{18}O_{prec}$ values estimated from soil nodules are within error of the modern value at Zagreb, and these minor variations can equally be explained by rainfall source shifts, temperature and evaporation effects during the summer season.

Author contributions

GÚ designed the study, performed field work and sampling with BB and wrote the paper. Stable and clumped isotope analyses were done by SK, supervised by SB. LH provided meteorological data, ÁN performed feldspar pIR-IRSL measurements. All co-authors contributed to the discussion/interpretation of results.

Conflict of interest

The authors declare no conflict of interest.

Acknowledgements

This work was funded by the National Research, Development and Innovation Office in Hungary (NKFI Alap KH-125584 project). Additional financial support provided by the Bolyai János Research Scholarship of the Hungarian Academy of Sciences (to GÚ) is gratefully acknowledged. The research was supported by the European Union and the State of Hungary, co-financed by the European Regional Development Fund in the project of GINOP-2.3.2-15-2016-00009 'ICER'. Constructive and insightful comments made by two anonymous reviewers greatly improved the paper.

Data availability

Supplementary text and datasets related to this article can be found at https://data.mendeley.com/submissions/evise/edit/6yhgmt4m25?submission_id=S0031-0182(18)30627-8&token=7b8e894c-5c81-46fc-a484-0b9ad11a7b78,

an open-source online data repository hosted at Mendeley Data.

References

Antoine, P., Rousseau, D.-D., Degeai, J.P., Moine, O., Lagroix, F., Kreutzer, S., Fuchs, M., Hatté, C., Gauthier, C., Svoboda, J., Lisá, L., 2013. High-resolution record of the environmental response to climatic variations during the Last Interglacial–Glacial cycle in Central Europe: the loess–paleosol sequence of Dolní Věstonice (Czech Republic). Quat. Sci. Rev. 67, 17–38.

Bakker, P., Stone, E.J., Charbit, S., Gröger, M., Krebs-Kanzow, U., Ritz, S.P., Varma, V., Khon, V., Lunt, D.J., Mikolajewicz, U., Prange, M., Renssen, H., Schneider, B., Schulz, M., 2013. Last interglacial temperature evolution – a model inter-comparison. Clim. Past 9, 605−619.

Barta, G., Bradák, B., Novothny, Á., Markó, A., Szeberényi, J., Kiss, K., Kovács, J., 2018. The influence of paleogeomorphology on the stable isotope signals of paleosols. Geoderma 330, 221–231.

Behre, K.-E., Hölzer, A., Lemdahl, G., 2005. Botanical macro-remains and insects from the Eemian and Weichselian site of Oerel (northwest Germany) and their evidence for the history of climate. Veg. Hist. Archaeobot. 14, 31–53.

Bernasconi, S.M., Hu, B., Wacker, U., Fiebig, J., Breitenbach, S.F.M., Rutz, T., 2013. Background effects on Faraday collectors in gas source mass spectrometry and implications for clumped isotope measurements. Rapid Commun. Mass Spectrom. 27, 603-612.

Bernasconi, S.M., Müller, I.A., Bergmann, K.D., Breitenbach, S.F.M., Fernandez, A., Hodell, D.A., Jaggi M., Meckler, A.N.,Millan, I., Ziegler, M., 2018. Reducing uncertainties in carbonate clumped isotope analysis through consistent carbonate-based standardization. Geochem. Geophy. Geosy. 19, https://doi.org/10.1029/2017GC007385.

Bradák, B., Thanó-Bozsó, E., Kovács, J., Márton, E., Csillag, G., Horváth, E., 2011. Characteristics of Pleistocene climate cycles identified in Cérna Valley loess-paleosol section (Vértesacsa, Hungary). Quat. Int. 234, 86–97.

Boch, R., Cheng, H., Spötl, C., Edwards, R.L., Wang, X., Häuselmann, P., 2011. NALPS: a precisely dated European climate record 120–60 ka. Clim. Past 7, 1247–1259.

Breecker, D.O., Sharp, Z.D., McFadden, L.D., 2009. Seasonal bias in the formation and stable isotopic composition of pedogenic carbonate in modem soils from Central New Mexico, USA. Geol. Soc. Am. Bull. 121, 630–640.

Breitenbach, S.F.M., Mleneck-Vautravers, M.J., Grauel, A.-L., Lo, L., Bernasconi, S.M., Müller, I.A., Rolfe, J., Gázquez, F., Greaves, M., Hodell, D.A., 2018. Coupled Mg/Ca and clumped isotope analyses of foraminifera provide consistent water temperatures. Geochim. Cosmochim. Acta, https://doi.org/10.1016/j.gca.2018.03.010.

Buggle, B., Hambach, U., Glaser, B., Gerasimenko, N., Marković, S.B., Glaser, I., Zöller, L., 2009. Stratigraphy and spatial and temporal paleoclimatic trends in East European loess paleosol sequences. Quaternary International 196, 86–106.

Buggle, B., Hambach, U., Kehl, M., Zöller, L., Marković, S.B., Glaser, B., 2013. The progressive evolution of a continental climate in SE-Central European lowlands during the Middle Pleistocene recorded in loess paleosol sequences. Geology 41, 771–774.

Buggle, B., Hambach, U., Müller, K., Zöller, L., Markovic, S. B., Glaser, B., 2014. Iron mineralogical proxies and quaternary climate change in SE European loess–paleosol sequences. Catena 117, 4–22.

Burgener, L., Huntington, K.W., Hoke, G.D., Schauer, A., Ringham, M.C., Latorre, C., Díaz, F.P., 2016. Variations in soil carbonate formation and seasonal bias over >4 km of relief in the western Andes (30ºS) revealed by clumped isotope thermometry. Earth Planet. Sci. Lett. 441, 188–199.

Burgener, L., Huntington, K.W., Sletten, R., Watkins, J.M., Quade, J., Hallet B., 2018. Clumped isotope constraints on equilibrium carbonate formation and kinetic isotope effects in freezing soils. Geochim. Cosmochim. Acta 235, 402−430.

Buylaert, J.-P., Jain, M., Murray, A.S., Thomsen, K.J., Jain, M., 2009. Testing the potential of an elevated temperature IRSL signal from K-feldspar. Radiat. Meas. 44, 560−565.

CAPE-Last Interglacial Project Members, 2006. Last Interglacial Arctic warmth confirms polar amplification of climate change. Quat. Sci. Rev. 25, 1383–1400.

Capron, E., Govin, A., Stone, E. J., Masson-Delmotte, V., Mulitza, S., Otto-Bliesner, B., Rasmussen, T. L., Sime, L. C., Waelbroeck, C., Wolff, E. W., 2014. Temporal and spatial structure of multi-millennial temperature changes at high latitudes during the Last Interglacial. Quat. Sci. Rev. 103, 116−133.

Cerling, T.E., 1984. The stable isotopic composition of modern soil carbonate and its relationship to climate. Earth Planet. Sci. Lett. 71, 229–240.

Cerling, T.E., Quade, J., 1993. Stable carbon and oxygen isotopes in soil carbonates, in: Swart, P.K., Lohmann, K.C., McKenzie, J., Savin, S. (Eds.), Climate Change in Continental Isotopic Records. Geophysical Monograph, Vol. 78. AGU, pp. 217–231.

Cheddadi, R., Mamakova, K., Guiot, J., de Beaulieu, J.-L., Reille, M., Andrieu, V., Granoszewski, W., Peyron, O., 1998. Was the climate of the Eemian stable? A quantitative climate reconstruction from seven European pollen records. Palaeogeogr. Palaeoclimatol. Palaeoecol. 143, 73–85.

Coplen, T.B., 1994. Reporting of stable hydrogen, carbon, and oxygen isotopic abundances (Technical Report). Pure Appl. Chem. 66, 273–276.

Daëron M., Blamart D., Peral M., Affek H. P., 2016. Absolute isotopic abundance ratios and the accuracy of Δ_{47} measurements. Chem. Geol. 442, 83-96.

Dearing, J.A., Dann, R.J.L., Hay, K., Lees, J.A., Loveland, P.J., Maher, B.A., Ogrady, K., 1996. Frequency-dependent susceptibility measurements of environmental materials. Geophys. J. Int. 124, 228–240.

Dennis, K.J., Affek, H.P., Passey, B.H., Schrag, D.P., Eiler J.W., 2011. Defining an absolute reference frame for ‘clumped’ isotope studies of CO_2. Geochim. Cosmochim. Acta 75, 7117–7131.

Dworkin, S.I., Nordt, L., Atchley, S., 2005. Determining terrestrial paleotemperatures using the oxygen isotopic composition of pedogenic carbonate. Earth Planet. Sci. Lett. 237, 56−68.

Eagle, R.A., Risi, C., Mitchell, J.L., Eiler, J.M., Seibt, U., Neelin, J.D., Li, G., Tripati, A.K., 2013. High regional climate sensitivity over continental China constrained by glacial-recent changes in temperature and the hydrological cycle. Proc. Natl. Acad. Sci. U. S. A. 110, 8813−8818.

Eiler, J.M., 2007. ‘‘Clumped-isotope’’geochemistry−the study of naturally-occurring, multiply-substituted isotopologues. Earth Planet. Sci. Lett. 262, 309–327.

Eiler, J.M., 2011. Paleoclimate reconstructions using carbonate clumped isotope thermometry. Quat. Sci. Rev. 30, 3575–3588.

EPICA community members, 2004. Eight glacial cycles from an Antarctic ice core. Nature, 429, 623–628.

Fitzsimmons, K.E., Marković, S.B., Hambach, U., 2012. Pleistocene environmental dynamics recorded in the loess of the middle and lower Danube Basin. Quat. Sci. Rev. 41, 104–118.

Forster, T., Evans, M.E., Heller, F., 1994. The frequency dependence of low field susceptibility in loess sediments. Geophys. J. Int. 118, 636–642.

Gallagher, T.M., Sheldon, N.D., 2016. Combining soil water balance and clumped isotopes to understand the nature and timing of pedogenic carbonate formation. Chem. Geol. 435, 79−91.

Galovic, L., 2014. Geochemical archive in the three loess/paleosol sections in the Eastern Croatia: Zmajevac I, Zmajevac and Erdut. Aeolian Res. 15, 113−132.

Ghosh, P., Adkins, J., Affek, H., Balta, B.,Guo, W., Schauble, E., Schrag, D., Eiler, J., 2006. 13C–18O bonds in carbonate minerals: a new kind of paleothermometer. Geochim. Cosmochim. Acta 70, 1439–1456.

Granoszewski, W., 2003. Late Pleistocene vegetation history and climatic changes at Horoszki Duże, Eastern Poland: a palaeobotanical study. Acta Palaeobot. Suppl. 4, 3–95.

Guiot, J., Reille, M., de Beaulieu, J.-L., Pons, A., 1992. Calibration of the climatic signal in a new pollen sequence from La Grande Pile. Clim. Dynam. 6, 259–264.

Guiot, J., de Beaulieu, J.-L., Cheddadi, R., David, F., Ponel, P., Reille, M., 1993. The climate in Western Europe during the last Glacial/Interglacial cycle derived from pollen and insect remains. Palaeogeogr. Palaeoclimatol. Palaeoecol. 103, 73–93.

Harrison, S.P., Kutzbach, J.E., Prentice, I.C., Behling, P.J., Sykes, M.T., 1995. The response of Northern Hemisphere extratropical climate and vegetation to orbitally induced changes in insolation during the Last Intergaciation. Quat. Res. 43, 174−184.

Heller, F., Shen, C.D., Beer, J., Liu, X.M., Liu, T.S., Bronger, A., Suter, M., Bonani, G., 1993. Quantitative estimations of pedogenic ferrimagnetic formation in Chinese loess and palaeoclimatic implications. Earth Planet. Sci. Lett. 114, 385–390.

Helmens, K.F., 2014. The Last Interglacial-Glacial cycle (MIS 5-2) re-examined based on long proxy records from central and northern Europe. Quaternary. Sci. Rev. 86, 115–143.

Hillel, D., 2003. Introduction to Environmental Soil Physics. Academic Press.

Hošek, J., Hambach, U., Lisá, L., Grygar, T.M., Horáček, I., Meszner, S., Knésl, I., 2015. An integrated rock-magnetic and geochemical approach to loess/paleosol sequences from Bohemia and Moravia (Czech Republic): Implications for the Upper Pleistocene paleoenvironment in central Europe. Palaeogeogr. Palaeoclimatol. Palaeoecol. 418, 344–358.

Hough, B.G., Fan, M., Passey, B.H., 2014. Calibration of the clumped isotope geothermometer in soil carbonate in Wyoming and Nebraska, USA: implications for paleoelevation and paleoclimate reconstruction. Earth Planet. Sci. Lett. 391, 110–120.

Huntington, K.W., Lechler, A.R., 2015. Carbonate clumped isotope thermometry in continental tectonics. Tectonophysics 647–648, 1–20.

Kaspar, F., Kühl, N., Cubasch, U., Litt, T., 2005. A model-data comparison of European temperatures in the Eemian interglacial. Geophys. Res. Lett. 32, L11703, doi: 10.1029/2005GL022456.

Kele, S., Breitenbach, S.F.M., Capezzuoli, E., Nele Meckler, A., Ziegler, M., Millan, I.M., Kluge, T., Deák, J., Hanselmann, K., John, C.M., Yan, H., Liu, Z., Bernasconi, S.M. 2015. Temperature dependence of oxygen- and clumped isotope fractionation in carbonates: a study of travertines and tufas in the 6–95 °C temperature range. Geochim. Cosmochim. Acta 168, 172–192.

Kim, S-T., O'Neil, J.R., 1997. Equilibrium and nonequilibrium oxygen isotope effects in synthetic carbonates. Geochim. Cosmochim. Acta 61, 3461–3475.

Kindler, P., Guillevic, M., Baumgartner, M., Schwander, J., Landais, A., Leuenberger, M., 2014. Temperature reconstruction from 10 to 120 kyr b2k from the NGRIP ice core. Clim. Past. 10, 887–902.

Klotz, S., Müller, U., Mosbrugger, V., de Beaulieu, J.-L., Reille, M., 2004. Eemian to early Würmian climate dynamics: history and pattern of changes in Central Europe. Palaeogeogr. Palaeoclimatol. Palaeoecol. 211, 107–126.

Koltai, G., Spötl, C., Shen, C.-C., Wu, C.-C., Rao, Z., Palcsu, L., Kele, S., Surányi, G., Bárány-Kevei, I., 2017. A penultimate glacial climate record from southern Hungary. J. Quaternary Sci. 32, 946–956.

Kopp, R. E., Simons, F. J., Mitrovica, J. X., Maloof, A. C., Oppenheimer, M., 2009. Probabilistic assessment of sea level during the last interglacial stage. Nature 462, 863–867.

Königer, P., Barta, G., Thiel, C., Bajnóczi, B., Novothny, Á., Horváth, E., Techmer, A., Frechen, M., 2014. Stable isotope composition of bulk and secondary carbonates from the Quaternary loess-paleosol sequence in Süttő, Hungary. Quat. Int. 319, 38–49.

Kühl, N., Litt, T., Schölzel, C., Hense, A., 2007. Eemian and Early Weichselian temperature and precipitation variability in northern Germany. Quaternary Sci. Rev. 26, 3311–3317.

Lisiecki, L. E., Raymo, M. E., 2005. A Pliocene-Pleistocene stack of 57 globally distributed benthic $\delta^{18}O$ records. Paleoceanography 20, PA1003, doi:10.1029/2004PA001071.

Liu, Q.S., Roberts, A.P., Larrasoana, J.C., Banerjee, S.K., Guyodo, Y., Tauxe, L., Oldfield, F., 2012. Environmental magnetism: principles and applications. Rev. Geophys. 50, RG4002.

Loulergue, L., Schilt, A., Spahni, R., Masson-Delmotte, V., Blunier, T., Lemieux, B., Barnola, J.-M., Raynaud, D., Stocker, T. F., Chappellaz, J., 2008. Orbital and millennial-scale features of atmospheric CH4 over the past 800,000 years. Nature 453, 383–386.

Lunt, D. J., Abe-Ouchi, A., Bakker, P., Berger, A., Braconnot, P., Charbit, S., Fischer, N., Herold, N., Jungclaus, J. H., Khon, V. C., Krebs-Kanzow, U., Langebroek, P. M., Lohmann, G., Nisancioglu, K. H., Otto-Bliesner, B., Park, W., Pfeiffer, M., Phipps, S. J., Prange, M., Rachmayani, R., Renssen, H., Rosenbloom, N., Schneider, B., Stone, E. J., Takahashi, K., Wei, W., Yin, Q., Zhang Z. S., 2013. A multi-model assessment of last interglacial temperatures. Clim. Past 9, 699–717.

Lüthi, D., Le Floch, M., Bereiter, B., Blunier, T., Barola, J. M., Siegenthaler, U., Raynaud, D., Jouzel, J., Fischer, H., Kawamura, K., Stocker, T. F., 2008. High-resolution carbon dioxide concentration record 650,000–800,000 years before present. Nature 453, 379–382.

Maher, B.A., 1986. Characterisation of soils by mineral magnetic measurements. Phys. Earth Planet. Inter. 42, 76–92.

Maher, B.A., Taylor, R.M., 1988. Formation of ultrafine-grained magnetite in soils. Nature 336, 368–370.

Maher, B.A., Thompson, R., 1995. Paleorainfall reconstructions from pedogenic magnetic susceptibility variations in the Chinese loess and paleosols. Quat. Res. 44, 383–391.

Maher, B.A., Thompson, R., Zhou, L.P., 1994. Spatial and temporal reconstructions of changes in the Asian palaeomonsoon: A new mineral magnetic approach. Earth Planet. Sci. Lett. 125, 461−471.

Marković, S.B., Hambach, U., Stevens, T., Kukla, G.J., Heller, F., McCoy, W.D., Oches, E.A., Buggle, B., Zöller, L., 2011. The last million years recorded at the Stari Slankamen loess-palaeosol sequence: revised chronostratigraphy and long-term environmental trends. Quat. Sci. Rev. 30, 1142−1154.

Marković, S.B., Sümegi, P., Stevens, T., Schaetzl, R.J., Obreht, I., Chu, W., Buggle, B., Zech, M., Zech, R., Zeeden, C., Gavrilov, M.B., Perić, Z., Svirčev, Z., Lehmkuhl, F., 2018. The Crvenka loess-paleosol sequence: A record of continuous grassland domination in the southern Carpathian Basin during the Late Pleistocene. Palaeogeogr. Palaeoclimatol. Palaeoecol. 509, 33–46.

McKay, N. P., Overpeck, J. T., Otto-Bliesner, B. L., 2011. The role of ocean thermal expansion in Last Interglacial sea level rise. Geophys. Res. Lett., 38, L14605, doi:10.1029/2011GL048280.

McManus, J.F., Bond, G.C., Broecker, W.S., Johnsen, S., Labeyrie, L., Higgins, S., 1994. High resolution climate records from the North-Atlantic during the last interglacial. Nature 371, 326–329.

Meckler, A. N., Ziegler, M., Millán, M. I., Breitenbach, S. F. M., Bernasconi, S. M., 2014. Long-term performance of the Kiel carbonate device with a new correction scheme for clumped isotope measurements. Rapid Commun. Mass Spectrom. 28(15), 1705-1715.

Müller, I.A., Fernandez, A., Radke, J., van Dijk, J., Bowen, D., Schwieters, J., Bernasconi, S.M., 2017. Carbonate clumped isotope analyses with the long-integration dual-inlet (LIDI) workflow: scratching at the lower sample weight boundaries. Rapid Commun. Mass Spectrom. 31, 1057–1066.

NEEM community members, 2013. Eemian interglacial reconstructed from a Greenland folded ice core. Nature 493, 489−494.

Nikolova, I., Yin, Q., Berger, A., Singh, U. K., Karami, M. P., 2013. The last interglacial (Eemian) climate simulated by LOVECLIM and CCSM3. Clim. Past 9, 1789−1806.

Novothny, Á., Frechen, M., Horváth, E., Wacha, L., Rolf, C., 2011. Investigating the penultimate and last glacial cycles of the Sütto loess section (Hungary) using luminescence dating, high-resolution grain size, and magnetic susceptibility data. Quaternary International 234 (1–2), 75–85.

Obreht, I., Zeeden, C., Hambach, U., Veres, D., Marković, S.B., Bösken, J., Svirčev, Z., Bačević, N., Gavrilov, M.B., Lehmkuhl, F., 2016. Tracing the influence of Mediterranean climate on Southeastern Europe during the past 350,000 years. Sci. Rep. 6, 36334, doi: 10.1038/srep36334.

Oppo, D.W., McManus, J.F., Cullen, J.L., 2006. Evolution and demise of the last Interglacial warmth in the subpolar North Atlantic. Quaternary Sci. Rev. 25, 3268–3277.

Otto-Bliesner, B.L., Rosenbloom, N., Stone, E.J., McKay, N.P., Lunt, D.J., Brady, E.C., Overpeck, J.T., 2013. How warm was the last interglacial? New model–data comparisons. Phil. Trans. R. Soc. A 371, 20130097.

Panaiotu, C.G., Panaiotu, C.E., Grama, A., Necula, C., 2001. Paleoclimatic record from a loess-paleosol profile in southeastern Romania. Phys. Chem. Earth (A) 26, 893–898.

Passey, B.H., Levin, N.E., Cerling, T.E., Brown, F.H., Eiler, J.M., 2010. High-temperature environments of human evolution in East Africa based on bond ordering in paleosol carbonates. Proc. Natl. Acad. Sci. U. S. A. 107, 11245–11249.

Past Interglacials Working Group of PAGES, 2016. Interglacials of the last 800,000 years. Rev. Geophys. 54, doi:10.1002/2015RG000482.

Peters, N.A., Huntington, K.W., Hoke, G.D., 2013. Hot or not? Impact of seasonally variable soil carbonate formation on paleotemperature and O-isotope records from clumped isotope thermometry. Earth Planet. Sci. Lett. 361, 208–218.

Peterse, F., Prins, M.A., Beets, C.J., Troelstra, S.R., Zheng, H., Gu, Z., Schouten, S., Sinninghe Damsté, J.S., 2011. Decoupled warming and monsoon precipitation in East Asia over the last deglaciation. Earth Planet. Sci. Lett. 301, 256–264.

Quade, J., Eiler, J., Daëron, M., Achyuthan, H., 2013. The clumped isotope geothermometer in soil and paleosol carbonate. Geochim. Cosmochim. Acta 105, 92–107.

Rasmussen, S.O., Bigler, M., Blockley, S.P., Blunier, T., Buchardt, S.L., Clausen, H.B., Cvijanovic, I., Dahl-Jensen, D., Johnsen, S.J., Fischer, H., Gkinis, V., Guillevic, M., Hoek, W.Z., Lowe, J.J., Pedro, J.B., Popp, T., Seierstad, I.K., Steffensen, J.P., Svensson, A.M., Vallelonga, P., Vinther, B.M., Walker, M.J.C., Wheatley, J.J., Winstrup, M., 2014. A stratigraphic framework for abrupt climatic changes during the Last Glacial period based on three synchronized Greenland ice-core records: refining and extending the INTIMATE event stratigraphy. Quat. Sci. Rev. 106, 14–28.

Ringham, M.C., Hoke, G., Huntington, K., Aranibar, J., 2016. Influence of vegetation type and site-to-site variability on soil carbonate clumped isotope records, Andean piedmont of Central Argentina (32–34ºS). Earth Planet. Sci. Lett. 440, 1–11.

Sánchez Goñi, M.F., 2007. Introduction to climate and vegetation in Europe during MIS5, in: Sirocko, F., Claussen, M., Sánchez Goñi, M.F., Litt, T. (Eds), The climate of past interglacials. Amsterdam: Elsevier. Developments in Quaternary Sciences 7, pp. 197–205.

Schauer, A.J., Kelson, J., Saenger, C., Huntington, K.W., 2016. Choice of ^{17}O correction affects clumped isotope (Δ_{47}) values of CO_2 measured with mass spectrometry. Rapid Commun. Mass Spectrom. 30, 2607–2616.

Schmid, T. W., Bernasconi. S. M., 2010. An automated method for 'clumped-isotope' measurements on small carbonate samples. Rapid Commun. Mass Spectrom. 24, 1955.

Schreuder, L.T., Beets, C.J., Prins, M.A., Hatté, C., Peterse, F., 2016. Late Pleistocene climate evolution in Southeastern Europe recorded by soil bacterial membrane lipids in Serbian loess. Palaeogeogr. Palaeoclimatol. Palaeoecol. 449, 141–148.

Shakun, J.D., Lea, D.W., Lisiecki, L.E., Raymo, M.E., 2015. An 800-kyr record of global surface ocean $\delta^{18}O$ and implications for ice volume-temperature coupling. Earth Planet. Sci. Lett. 426, 58–68.

Sprafke, T., Thiel, C., Terhorst, B., 2014. From micromorphology to palaeoenvironment: The MIS 10 to MIS 5 record in Paudorf (Lower Austria). Catena 117, 60−72.

Stevens, T., Marković, S.B., Zech, M., Hambach, U., Sümegi, P., 2011. Dust deposition and climate in the Carpathian Basin over an independently dated last glacial-interglacial cycle. Quat. Sci. Rev. 30, 662−681.

Sümegi, P., Gulyás, S., Molnár, D., Sümegi, B.P., Almond, P.C., Vandenberghe, J., Zhou, L., Pál-Molnár, E., Törőcsik, T., Hao, Q., Smalley, I., Molnár, M., Marsi, I., 2018. New chronology of the best developed loess/paleosol sequence of Hungary capturing the past 1.1 ma: Implications for correlation and proposed pan-Eurasian stratigraphic schemes. Quat. Sci. Rev. 191, 144−166.

Terhorst, B., Ottner, F., Wriessnig, K., 2012. Weathering intensity and stratigraphy of the Middle to Upper Pleistocene loess/palaeosol sequence of Wels-Aschet in Upper Austria. Quat. Int. 265, 142−154.

Thomsen, K.J., Murray, A.S., Jain, M., Bøtter-Jensen, L., 2008. Laboratory fading rates of various luminescence signals from feldspar-rich sediment extracts. Radiat. Meas. 43, 1474−1486.

Turney, C.S.M., Jones, R.T., 2010. Does the Agulhas Current amplify global temperatures during super-interglacials? J. Quaternary Sci. 25, 839−843.

Újvári, G., Mentes, Gy, Bányai, L., Kraft, J., Gyimóthy, A., Kovács, J., 2009. Evolution of a bank failure along the River Danube at Dunaszekcső, Hungary. Geomorphology 109, 197–209.

Újvári, G., Molnár, M., Novothny, Á., Páll-Gergely, B., Kovács, J., Várhegyi, A., 2014. AMS ^{14}C and OSL/IRSL dating of the Dunaszekcső loess sequence (Hungary): chronology for 20 to 150 ka and implications for establishing reliable age-depth models for the last 40 ka. Quat. Sci. Rev. 106, 140–154.

Wohlfarth, B., 2013. A review of Early Weichselian climate (MIS 5d-a) in Europe, Swedish Nuclear Fuel and Waste Management Co. Technical Report 13-03.

Worm, H.-U., 1998. On the superparamagnetic-stable single domain transition for magnetite, and frequency dependency of susceptibility. Geophys. J. Int. 133, 201–206.

Wu, J., Nofziger, D. L., 1999. Incorporating temperature effects on pesticide degradation into a management model. J. Environ. Qual. 28, 92−100.

Zech, R., Zech, M., Marković, S., Hambach, U., Huang, Y., 2013. Humid glacials, arid interglacials? Critical thoughts on pedogenesis and paleoclimate based on multi-proxy analyses of the loess–paleosol sequence Crvenka, Northern Serbia. Palaeogeogr. Palaeoclimatol. Palaeoecol. 387, 165–175.

Zeeden, C., Kels, H., Hambach, U., Schulte, P., Protze, J., Eckmeier, E., Marković, S.B., Klasen, N., Lehmkuhl, F., 2016. Three climatic cycles recorded in a loess-palaeosol sequence at Semlac (Romania) – implications for dust accumulation in south-eastern Europe. Quat. Sci. Rev. 154, 130–154.

Zhou, L.P., Oldfield, F., Wintle, A.G., Robinson, S.G., Wang, J.T., 1990. Partly pedogenic origin of magnetic variations in Chinese loess. Nature 346, 737–739.

Yin, Q. Z., Berger, A., 2012. Individual contribution of insolation and CO2 to the interglacial climates of the past 800,000 years. Clim. Dynam. 38, 709–724.

Figure captions

Figure 1. Location and general climatic data of the study site (red) and two meteorological stations (blue) in Hungary. Abbreviations: PET – potential evapotranspiration, MAT – mean annual air temperature, SAT – summer season (JJA) air temperature, MAP – mean annual precipitation.

Figure 2. Air/soil temperatures a) over the year and b) the relationship between mean summer air (2 m) and soil temperatures measured at 1, 0.5 and 0.2 m depths at the Szeged meteorological station. Data reported are averages of six consecutive years from 2005 to 2010. Soil temperatures were measured at 0.1, 0.2, 0.5 and 1.0 m depths, while air temperature at 2 m as indicated with a thick blue line in panel a). Linear equations shown in panel b) are Eq. (8), (9) and (10) in the main text (section 3.1).

Figure 3. Modeled and reconstructed soil temperatures (ST-Δ_{47sc}) a) and carbon/oxygen stable isotopic compositions b) of soil carbonates as a function of depth in the S1 paleosol at Dunaszekcső. The green line in panel a) is the best-fit summer season soil temperature curve (modeled - 0.4 ºC) for the soil carbonate Δ_{47} data, intersecting the soil surface at TºC$(47)_0$ = 22.0, being the "effective surface temperature" defined by Quade et al. (2013). Soil temperature modeling details are found in the Methods section. MAT is modern mean annual air temperature in ºC.

Figure 4. Seasonal oxygen isotope composition of precipitation as a function of air temperature at the Zagreb GNIP station from 1980 to 1995. The range of reconstructed $\delta^{18}O_{prec}$ values from soil carbonates (>1 m depth) are also shown.

Figure 5. Lithology A), Δ_{47}-based soil (ST-Δ_{47sc}, green dot) and calculated summer air temperatures (SAT, red dot) B), pedogenic magnetic susceptibilities (χ_P) and mean annual precipitation (MAP) C) as a function of depth in the Dunaszekcső loess-paleosol record. The sediment sequence was dated by the infrared stimulated luminescence (IRSL) method, and the given post-IR IRSL ages are reported in Table 3. Modern MAT and SAT as given in Figure 1. The brGDGT-based temperature range is from Schreuder et al. (2016). The LR04 benthic $\delta^{18}O$ record for MIS 5 D) (Lisiecki and Raymo, 2005), as a proxy of global ice volume and deep ocean temperature, is also shown and correlated with the pedogenic susceptibility (χ_P) record. Ages of MIS boundaries and sub-stage peaks after Lisieczki and Raymo (2005). Estimated summer sea surface temperatures (SSTs) from site ODP-980 in the subpolar North Atlantic (Oppo et al., 2006) and Greenland $\delta^{15}N$-based temperatures (Kindler et al., 2014), with potential correlations (dotted lines, Sánchez Goñi, 2007; Wohlfart, 2013), are also displayed. Greenland stadial/interstadial periods are after Rasmussen et al. (2014).

Table captions

Table 1. Soil carbonate stable and clumped isotopic compositions from the Dunaszekcső sequence S1 paleosol, and calculations of paleoenvironmental parameters

Table 2. Parameters for soil temperature modeling

Table 3. IRSL chronology of the S1 paleosol at Dunaszekcső

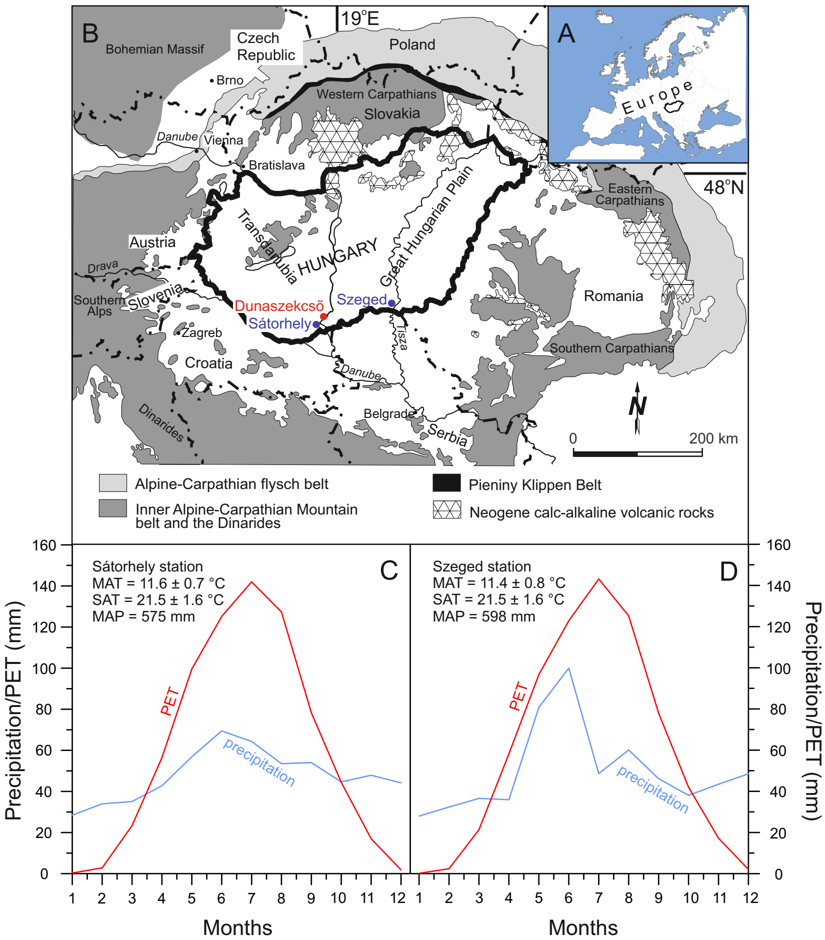

B
A
Europe
19°E
48°N
Bohemian Massif
Czech Republic
Poland
Brno
Western Carpathians
Slovakia
Danube
Vienna
Bratislava
Eastern Carpathians
Transdanubia
HUNGARY
Great Hungarian Plain
Austria
Drava
Southern Alps
Slovenia
Dunaszekcső
Szeged
Sátorhely
Zagreb
Croatia
Romania
Tisza
Southern Carpathians
Danube
Belgrade
Serbia
Dinarides
N
0
200 km
Alpine-Carpathian flysch belt
Inner Alpine-Carpathian Mountain belt and the Dinarides
Pieniny Klippen Belt
Neogene calc-alkaline volcanic rocks
Sátorhely station
MAT = 11.6 ± 0.7 °C
SAT = 21.5 ± 1.6 °C
MAP = 575 mm
C
PET
precipitation
Szeged station
MAT = 11.4 ± 0.8 °C
SAT = 21.5 ± 1.6 °C
MAP = 598 mm
D
PET
precipitation
Precipitation/PET (mm)
Months
Months
0
20
40
60
80
100
120
140
160
1
2
3
4
5
6
7
8
9
10
11
12

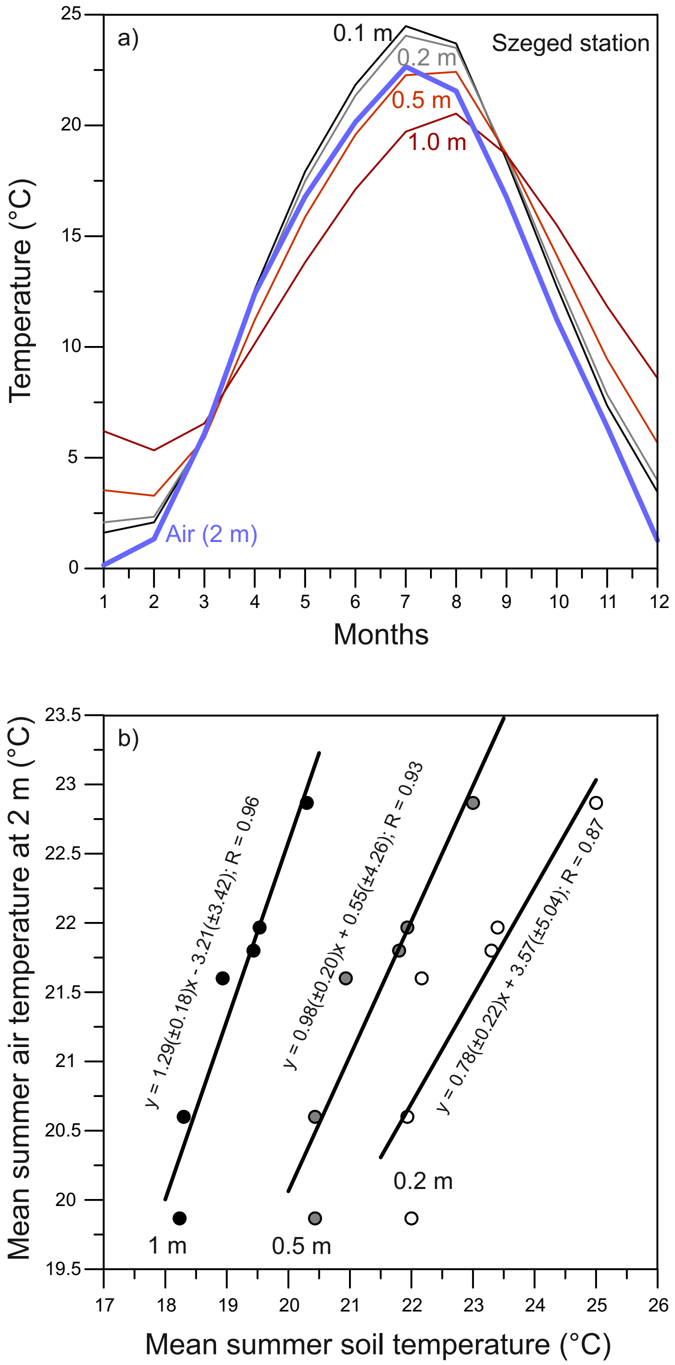
a)
Szeged station
0.1 m
0.2 m
0.5 m
1.0 m
Air (2 m)
Temperature (°C)
Months
b)
y = 1.29(±0.18)x - 3.21(±3.42); R = 0.96
y = 0.98(±0.20)x + 0.55(±4.26); R = 0.93
y = 0.78(±0.22)x + 3.57(±5.04); R = 0.87
1 m
0.5 m
0.2 m
Mean summer air temperature at 2 m (°C)
Mean summer soil temperature (°C)

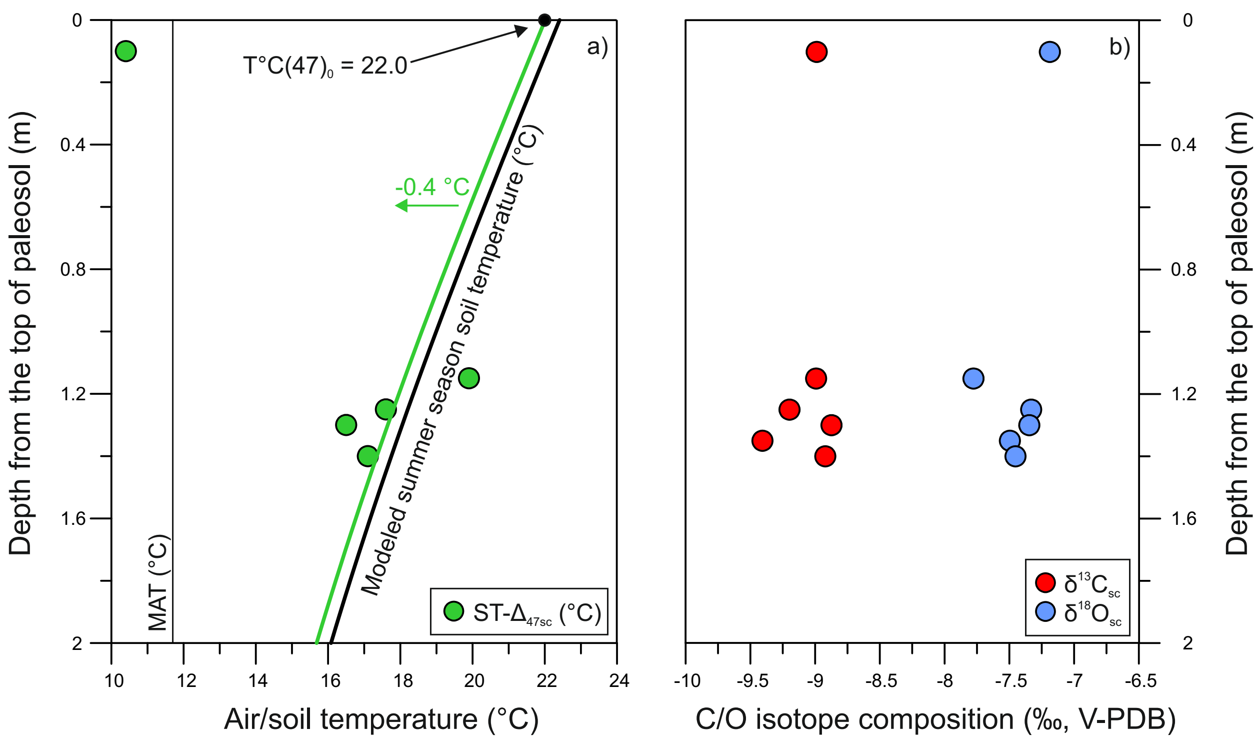

Depth from the top of paleosol (m)
0
0.4
0.8
1.2
1.6
2
T°C(47)0 = 22.0
-0.4 °C
Modeled summer season soil temperature (°C)
MAT (°C)
ST-Δ47sc (°C)
a)
10
12
14
16
18
20
22
24
Air/soil temperature (°C)
b)
δ13Csc
δ18Osc
-10
-9.5
-9
-8.5
-8
-7.5
-7
-6.5
C/O isotope composition (‰, V-PDB)

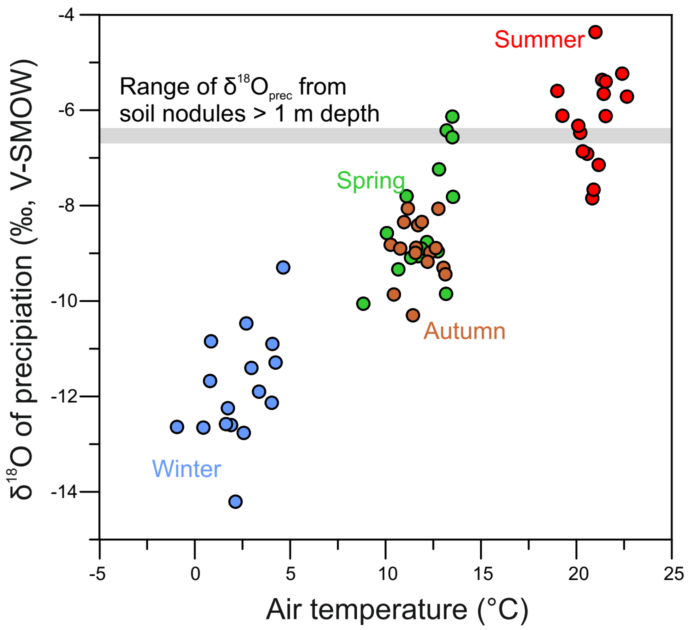

Summer
Range of $\delta^{18}O_{prec}$ from soil nodules > 1 m depth
Spring
Autumn
Winter
$\delta^{18}O$ of precipiation (‰, V-SMOW)
Air temperature (°C)

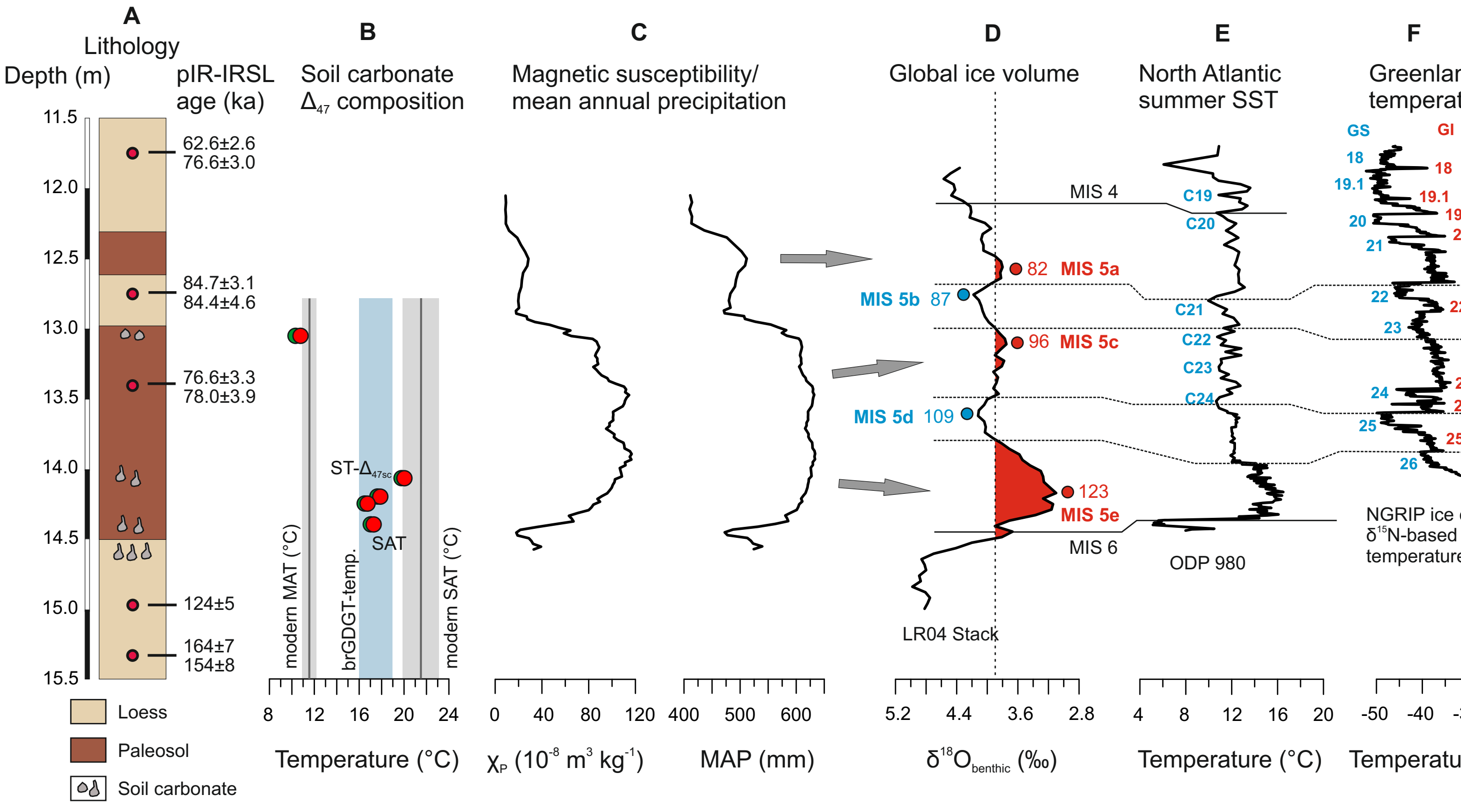

A
Lithology
Depth (m)
pIR-IRSL age (ka)
62.6±2.6
76.6±3.0
84.7±3.1
84.4±4.6
76.6±3.3
78.0±3.9
124±5
164±7
154±8
Loess
Paleosol
Soil carbonate
B
Soil carbonate Δ47 composition
modern MAT (°C)
brGDGT-temp.
ST-Δ47sc
SAT
modern SAT (°C)
Temperature (°C)
C
Magnetic susceptibility/ mean annual precipitation
χP (10^-8 m^3 kg^-1)
MAP (mm)
D
Global ice volume
MIS 4
82 MIS 5a
MIS 5b 87
96 MIS 5c
MIS 5d 109
123 MIS 5e
MIS 6
LR04 Stack
δ18Obenthic (‰)
E
North Atlantic summer SST
C19
C20
C21
C22
C23
C24
ODP 980
Temperature (°C)
F
Greenlar
temperat
GS
GI
NGRIP ice
δ15N-based
temperature
Temperatu

Table 1. Soil carbonate stable and clumped isotopic compositions from the Dunaszekcső sequence S1 paleosol, and calculations of paleoenvironmental parameters

Depth (m)	From soil surface (m)	Sample codes	Replicates	$\delta^{13}C_{sc}$ (V-PDB)	SE	$\delta^{18}O_{sc}$ (V-PDB)	SE	δ_{47}	Δ_{47} (‰)	SE	ST (ºC)[a]	±ST uncertainty (ºC)[b]	SAT_ 1 (ºC)[c]	SAT_ 0.5 (ºC)[c]	MAT (ºC)[d]	$\delta^{18}O_{prec}$ (V-SMOW)[e]	$\pm\delta^{18}O_{prec}$ uncertainty[f]
12.95-13.10	0-0.15	DSZ-SC-1	9	-8.99	0.02	-7.19	0.03	-2.148	0.725	0.005	10.4	1.3	10.3	10.8	11.1	-7.89	-0.03
14.00-14.15	1.05-1.20	DSZ-SC-8	8	-8.99	0.02	-7.78	0.03	-2.783	0.690	0.014	19.9	4.0	22.4	20.0	9.9	-6.45	-0.03
14.15-14.30	1.20-1.35	DSZ-SC-9/1	7	-9.20	0.02	-7.33	0.05	-2.507	0.698	0.011	17.6	3.1	19.5	17.8	10.9	-6.48	-0.05
14.15-14.30	1.20-1.35	DSZ-SC-9/2	9	-8.87	0.05	-7.35	0.08	-2.223	0.702	0.011	16.5	3.1	18.1	16.7	10.8	-6.72	-0.08
14.30-14.45	1.35-1.5	DSZ-SC-10/1	8	-9.41	0.02	-7.50	0.07	-2.843	0.757	0.007	2.7	1.7	0.3	3.2	10.5	-9.97	-0.07
14.30-14.45	1.35-1.5	DSZ-SC-10/3	7	-8.92	0.04	-7.45	0.05	-2.376	0.700	0.023	17.1	6.1	18.9	17.3	10.6	-6.70	-0.05

Abbreviations

[a]STs (soil temperatures) were calculated using the travertine Δ_{47}-temperature calibration by Kele et al. (2015), recalculated with the new Brandt parameters (Breitenbach et al., 2018; Bernasconi et al., 2018)

[b]Mean uncertainty of ST, calculated from the SE of Δ_{47} (calibration equation errors are not included)

[c]SATs (summer season air temperatures) for 1 and 0.5 m depth were calculated using Eqs. (8)-(9)

[d]MAT (mean annual air temperature) values were derived using T (ºC) = ($\delta^{18}O_{sc}$ (V-PDB) + 12.65)/0.49 (Dworkin et al., 2005)

[e]Paleoprecipitation oxygen isotopic compositions were calculated from $\delta^{18}O_{sc}$ and Δ_{47}-based ST data using the low-temperature calcite-water oxygen isotope fractionation equation of Kim and O'Neil (1997)
[f]Uncertainty of precipitation oxygen isotopic compositions was calculated by propagating standard errors of soil carbonate oxygen isotope values and does not include uncertainties associated with Δ_{47}-based temperature estimates

Table 2. Parameters for soil temperature modeling

Parameter	Value	Source
Average air temperature, T_{avg} (C°)	11.6	closest meteorological station
Annual amplitude of surface soil temperature, A_0	12	closest meteorological station
Thermal conductivity, κ (W/m*K)	1.7	Wu and Nofziger (1999)
Volumetric heat capacity, c_v (J/m3*K)	1800000	Wu and Nofziger (1999)
Thermal diffusivity, D_H (m2/s); $D_H = \kappa/c_v$	0.000000944	
Radial frequency, ω (2π/yr in seconds)	0.000000199	
Damping (1/e folding) depth, d (m); $d = (2D_H/\omega)^{1/2}$	3.079	
Soil depth, z (m)	0-2	

Table 3. IRSL chronology of the S1 paleosol at Dunaszekcső

Sample depth (m)	Sample code	Water content (%)	Dose rate (Gy/ka)	pIR IRSL 225 age (ka)	±1σ	pIR IRSL 290 age (ka)	±1σ	Source
11.75	Dsz-4	15±5	3.14±0.12	62.6	2.6	76.6	3.0	Újvári et al. (2014)
12.75	Dsz-5	20±5	3.02±0.11	84.7	3.1	84.4	4.6	Újvári et al. (2014)
13.40	Dsz-6	20±5	3.75±0.13	76.6	3.3	78.0	3.9	Újvári et al. (2014)
14.90	Dsz-6b	20±5	2.91±0.12			124.0	5.0	this study
15.35	Dsz-7	20±5	2.76±0.11	164.0	7.0	154.0	8.0	Újvári et al. (2014)